nature electronics

SUPPLEMENTARY INFORMATION

https://doi.org/10.1038/s41928-018-0055-7

In the format provided by the authors and unedited.

Near-quantum-limited amplification from inelastic Cooper-pair tunnelling

S. Jebari[1], F. Blanchet[1], A. Grimm[1], D. Hazra[1], R. Albert[1], P. Joyez[2], D. Vion[2], D. Estève[2], F. Portier[2] and M. Hofheinz[1,3]*

[1]Université Grenoble Alpes, CEA, INAC-PHELIQS, Grenoble, France. [2]SPEC, CEA, CNRS, Université Paris-Saclay, CEA-Saclay, Gif-sur-Yvette, France. [3]Institut Quantique and Département de génie électrique et de génie informatique, Université de Sherbrooke, Sherbrooke, Québec, Canada.
*e-mail: max.hofheinz@usherbrooke.ca

I. SAMPLE

The experiments shown in this work have been performed on a single sample shown in Supplementary Figure 1, the same as in [1]. It consists of an aluminium SQUID (see Supplementary Figure 1b) at the end of a stepped transmission line forming the resonator. The transmission line is etched from a Niobium layer on top of an oxidised silicon wafer. The length of each segment is adjusted to be a quarter wavelength at 6.0 GHz. The segment closest to the SQUID has a nominal characteristic impedance of $139\,\Omega$, the second segment of $25.5\,\Omega$. The rest of the circuit is 50 Ohm matched and forms a taper to connect the sample to a printed circuit board which connects it to a coax cable via a miniSMP connector. Seen from the junction, this stepped transmission line has a design input impedance with peaks at 6 GHz and odd multiples, as shown in Fig. 1c of the paper. Magnetic flux can enter the SQUID region via the transmission line and is applied via a flux coil below the sample.

II. GAIN, LOSS AND PARAMETRIC OSCILLATION ALONG THE ONE-PHOTON PROCESS

Along the line $\nu = f$ both gain (at $\nu \gtrapprox f$, label $\rhd 0\epsilon$) and loss (at $\nu \lessapprox f$, label $0{\lhd}\epsilon$) are visible in Fig. 2. They can be explained in the same way as the other gain and loss signatures, but they involve idler photons at very low frequency. Such processes are strong even though the impedance does not have a maximum at low frequency because the probability of photon emission scales with $\mathrm{Re}\,Z(f)/f$, so that processes involving low frequency photons are enhanced. The loss signature has here the same slope as the gain signature because the Cooper pair tunnels *against* the bias voltage.

This interpretation of the one-photon process as very asymmetric multi-photon process also explains the finite width of the noise signature $\rhd 0$ in Fig. 2: The low frequency thermal photons can add or remove energy, so that energy hf of the observed photon can be slightly different from the Cooper pair energy $2eV$. The voltage itself is then considered noiseless. In the paper we have, equivalently, included these low frequency thermal fluctuations in the bias voltage.

Around $\nu = 6$ GHz, $f = 6$ GHz, the noise signature in Fig. 2a and the gain signature in Fig. 2b fan out (indicated by label “po”). We attribute this effect to a parametric oscillation regime of the process described above [2]. Because of the $\mathrm{Re}\,Z(f)/f$ scaling, the threshold for parametric oscillation is reached much earlier for this process involving low frequency photons than for the desired process involving two photons at ≈ 6 GHz, even for low-frequency modes with very low quality factor.

III. ADDITIONAL SIGNATURES IN THE GAIN AND NOISE MEASUREMENTS

In addition to the processes we discuss in the paper, there is one additional line in Fig. 2a at $\nu = 15\,\mathrm{GHz} + f$. It corresponds to a spurious mode in our setup at 15 GHz, most likely formed by a standing wave between the microwave connector (miniSMP) connecting the sample-holder PCB to a microwave line and the end of our quarter-wave transformer. This spurious mode produces the signatures at $\nu = 15\,\mathrm{GHz} \pm f$ in Fig. 2c.

In Fig. 2c we also observe additional horizontal lines at $\nu = 15$ GHz and $\nu = 18$ GHz. We attribute these lines to enhanced phase noise in the reflected signal when the junction is on resonance with the designed 18 GHz mode or parasitic 15 GHz mode. According to its intensity, the process is of the same order in photon number as the amplification process, but the fact that it is horizontal indicates that it does not change signal photon number. It therefore involves a virtual photon at the signal frequency and a real photon at 18 GHz or 15 GHz. While this process does not change the photon number in the signal mode, it alters the phase of the reflected signal. Any modulation of the intensity of this process therefore leads to phase noise, which appears as loss in the phase-sensitive VNA measurement. The modulation of the intensity of this process arises from low-frequency voltage fluctuation exactly as in the case of excess noise with respect to the quantum limit in gain regions, as discussed in the paper.

IV. MICROWAVE NOISE MEASUREMENTS

The noise signal emitted by the sample is amplified and band-pass filtered into 4 to 8 GHz. It is then down-converted into a 1.1 to 1.9 GHz band-pass filter, matching the 2nd Nyquist band of a AlazarTech ATS9373 digitizer with 2 GS/s sampling rate. This setup permits us to measure power spectral density between 4 to 8 GHz with an instantaneous bandwidth of approximately 800 MHz using a small set of local oscillators between approximately 3 and 9 GHz.

A. Calibration

In order to calibrate PSD and VNA measurements, we place a Radiall R591763600 microwave switch (thermally anchored to the mixing chamber) between the bias-T and the chip (see Fig. 1). It connects the amplification chain either to the sample, to a short circuit or to two $50\,\Omega$ loads, one thermally anchored to the mixing chamber, one to the still. The well-known thermal noise (expressed in number of photons) emitted by the $50\,\Omega$ resistors is

$$N_{\mathrm{source}}(T,f) = \frac{1}{2}\left(\coth\left(\frac{hf}{2k_{\mathrm{B}}T}\right) - 1\right) \qquad \text{(S1)}$$

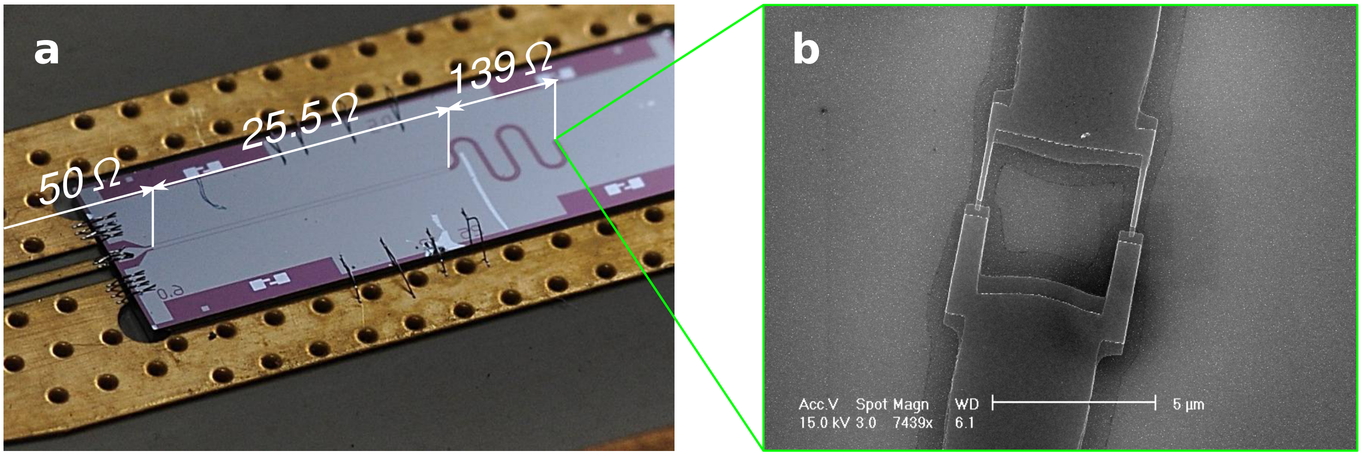

Supplementary Figure 1. **Sample. a,** Photograph of the sample in the sample holder. During measurement the sample holder is closed with a copper lid and a flux coil is placed below the sample holder to tune the SQUID. The chip measures $10\,\mathrm{mm} \times 3\,\mathrm{mm}$ **b,** Scanning electron micrograph of a SQUID with identical design as the one on the sample used in this work with nominal junction size $100\,\mathrm{nm} \times 100\,\mathrm{nm}$

in our impedance-matched setup. For $kT \ll hf$ the formula simplifies to $N \approx 0$ and for $kT \gg hf$ to $N \approx \frac{kT}{hf}$. Therefore, for the $50\,\Omega$ resistor anchored to the mixing chamber ($\frac{kT}{hf} \approx 0.04$), we get $N \approx 0$, so that its exact temperature is not essential. However, for the resistor thermally anchored to the still $\frac{kT}{hf} \approx 3$, so that N depends almost linearly on the exact temperature. To get an accurate temperature of this resistor we thermally decouple it from the microwave switch at mixing chamber temperature by a piece of NbTi superconducting coax cable and thermally anchor it to the still with a long copper strap. A germanium thermometer placed right next to the resistor tracks its temperature (typically 0.9 K).

The power spectral density D at the output of our measurement chain is

$$D = G(f)(N(f) + N_{\mathrm{source}}(T, f)) \tag{S2}$$

where $G(f)$ is the gain of the chain and $N(f)$ the system noise temperate. From a measurement of D for the two loads at different temperature, with N_{source} known from Eq. (S1), we extract the gain and noise of the measurement chain for each frequency (see Supplementary Figure 2).

V. GAIN MEASUREMENTS

Gain measurements are performed using an Agilent E5071C vector network analyser as shown in Fig. 1.

A. Gain calibration

We have two possibilities for normalising VNA measurements: They can be normalised with respect to the reflection off the short circuit on the microwave switch (see above) or with respect to reflection off the sample, for a set of parameters where it produces negligible gain or loss: We first choose a voltage where gain is close to 1 in Fig. 2 and then fully frustrate the SQUID to completely suppress any residual gain or loss. We observe very similar attenuation with both calibration techniques, indicating that loss between the microwave switch and the junction is negligible. However, the frequency dependence is not exactly the same due to parasitic reflections in the cable connecting the switch to the sample. We, therefore, use the latter calibration which cancels these modulations. This means, we show the intrinsic gain of the sample chip, not of the full device including chip, sample holder and the line to the microwave switch.

B. Input power calibration

This calibration technique compensates the combined transmission coefficient of the input and output line. However, for gain compression measurements shown in Fig. 4 we must know the input attenuation separately in order to accurately determine the power sent to the device. To do so we connect the switch to the short circuit, reflecting the input signal and sending it to the already calibrated power spectral density measurement (see above). Integration over the peak in power spectral density (using a flattop window function) and dividing by the gain of the PSD measurement gives us the power sent to the device.

VI. INPUT ADDED NOISE OF THE ICTA

The output noise of the ICTA is measured as the difference between the noise the sample emits at bias ν and at bias 0. It measures photon emission, i.e. it removes

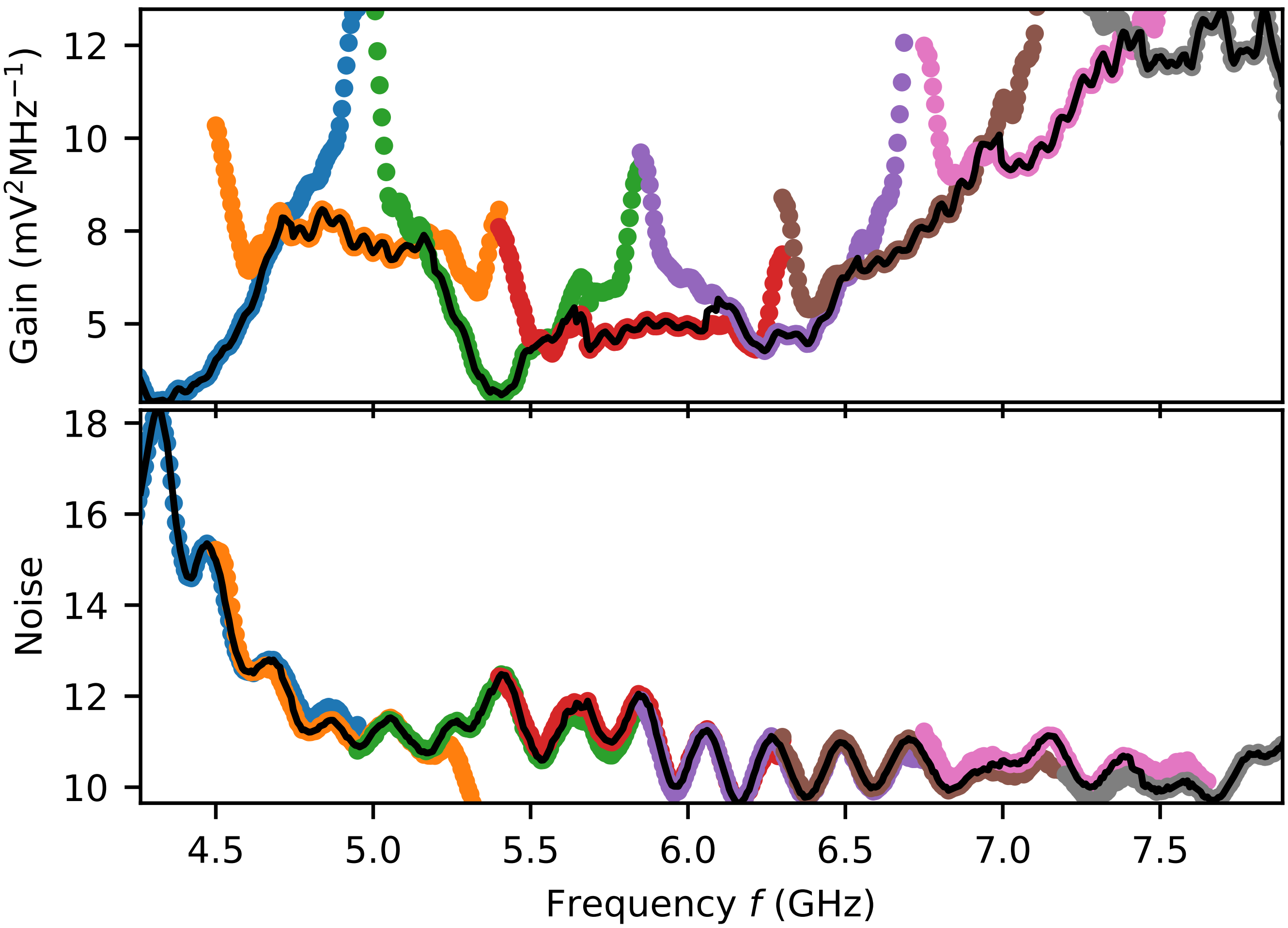

Supplementary Figure 2. **Calibration of the amplification chain.** Measuring the power spectral density at the output of our amplification chain for 2 different noise references (see text) allows us to determine the gain and noise in photons of the chain for each frequency. Calibration measurements are performed for different local oscillators used in the experiment (coloured dots). The frequency ranges covered by different local oscillators overlap and for each frequency we choose the local oscillator giving lowest aliasing and mixer spur terms. The solid black curve gives the gain and noise retained for each frequency. Note that at a given frequency the gain for different local oscillators can differ significantly but that the noise is the same (except at the very edge of each band where aliasing and for some ranges mixer spur terms become important), indicating that noise is dominated by amplification before the mixer.

noise added by the amplification chain and zero-point fluctuation. We therefore calculate the noise added by the sample as

$$n_{\mathrm{in}} = \frac{n_{\mathrm{out}} + 1/2}{G} - \frac{1}{2} = \frac{n_{\mathrm{out}}}{G} - \frac{1}{2}\left(1 - \frac{1}{G}\right) \tag{S3}$$

when it achieves a power gain G.

VII. CRITICAL CURRENT

Critical currents in the 10 nA range are very hard to measure accurately because current noise will make the junction leave the currant branch below the actual critical current. We therefore evaluate the nominal critical current as 17.5 nA from prior measurements of the normal state resistance at 4 K and an estimated gap of $2\Delta = 0.2$ meV of our Aluminium junction using the Ambegaokar-Baratoff formula. The agreement with the critical current 20.2 nA obtained from fitting the gain signature is remarkably good given that we operate in a regime where Eq. (2) of the Methods is not strictly valid.

VIII. EFFECTIVE TEMPERATURE OF THE ELECTROMAGNETIC ENVIRONMENT OF THE SAMPLE

In order to estimate the effective temperature of the low-frequency electromagnetic environment we perform a PSD measurement similar to Fig. 2 but at almost fully frustrated SQUID where Eq. (2) of the Methods is valid.

We perform the integral

$$\int_{4\,\mathrm{GHz}}^{8\,\mathrm{GHz}} \mathrm{d}f \gamma(\delta\nu + f, f) \propto P(h\delta\nu) \tag{S4}$$

for small $\delta\nu$, i.e. around the 1-photon process. It allows us to evaluate $P(h\delta\nu)$ around 0, which we fit with an effective temperature $T_{\text{eff}} = 54.7\,\text{mK}$. We neglect here the second term in Eq. (2) of the Methods: After integration it would lead to a smooth background which we find to be negligible, in agreement with $e^{-hf_0/kT_{\text{eff}}} \approx 0.005 \ll 1$.

[1] Hofheinz, M. *et al.* Bright side of the Coulomb blockade. *Phys. Rev. Lett.* **106**, 217005 (2011).

[2] Cassidy, M. C. *et al.* Demonstration of an ac Josephson junction laser. *Science* **355**, 939–942 (2017).